Journal of The Electrochemical Society, **161** (5) F668-F673 (2014)
0013-4651/2014/161(5)/F668/6/$31.00 © The Electrochemical Society

Enhancing Sulfur Tolerance of a Ni-YSZ Anode through $BaZr_{0.1}Ce_{0.7}Y_{0.1}Yb_{0.1}O_{3-\delta}$ Infiltration

Sivaprakash Sengodan,[a] Mingfei Liu,[b] Tak-Hyoung Lim,[c] Jeeyoung Shin,[d,z] Meilin Liu,[b,*] and Guntae Kim[a,z]

[a]*Interdisciplinary School of Green Energy, Ulsan National Institute of Science and Technology (UNIST), Ulsan 689-798, Korea*
[b]*School of Materials Science and Engineering, Georgia Institute of Technology, Atlanta, Georgia 30332, USA*
[c]*Fuel Cell Laboratory, New and Renewable Energy Research Division, Korea Institute of Energy Research, Daejeon 305-343, Korea*
[d]*Department of Mechanical Engineering, Dong-Eui University, Busan 614-714, Korea*

In this study, sulfur tolerance of a conventional Ni-yttria stabilized zirconia (Ni-YSZ) anode for solid oxide fuel cells is significantly improved by surface modification. The Ni-YSZ anode modified by the infiltration of $BaZr_{0.1}Ce_{0.7}Y_{0.1}Yb_{0.1}O_{3-\delta}$ (BZCYYb) demonstrates stable performance in a sulfur-containing H_2 fuel over 500 hours. In contrast, the bare Ni-YSZ anode without surface modification degrades drastically when exposed to the sulfur-containing H_2 fuel. This implies that the BZCYYb coating is an excellent catalyst for surface modification of the conventional Ni-YSZ anode. A single step infiltration of BZCYYb into the Ni-YSZ anode was sufficient to provide good sulfur tolerance.
© 2014 The Electrochemical Society. [DOI: 10.1149/2.068405jes] All rights reserved.

Manuscript submitted January 16, 2014; revised manuscript received March 20, 2014. Published March 31, 2014.

Solid oxide fuel cells (SOFCs) are promising energy conversion devices due to their advantages such as fuel flexibility, high efficiency power generation, low emissions, and system compactness. In particular, hydrocarbon fueled SOFCs have received considerable attention due to the abundance and accessibility of fuel, which significantly reduces the cost of SOFC technologies.[1–3] Conventional SOFCs, which use a Ni-YSZ cermet anode and YSZ electrolyte, are commercially available with pure H_2 as fuel; but this Ni-YSZ anode, when operated on hydrocarbon fuels, is highly susceptible to coking and deactivation by other contaminants.[4,5] For example, hydrogen sulfide (H_2S), the most common impurity in reformed hydrocarbon fuels, can deteriorate the activity of conventional Ni-YSZ anode under SOFC operating conditions, even in parts per million (ppm) levels.[6–8] Most previous studies indicated that sulfur is strongly adsorbed on the Ni surface and blocks the triple phase boundaries for electrochemical oxidation of the fuel, which results in performance degradation due to the considerably increased anodic polarization.[9–11]

Efforts have thus been made to identify Ni free anode materials that provide improved sulfur tolerance and coking tolerance to operate on hydrocarbon fuels. Several anode materials including Sr_2MgMoO_6, $La_{1-x}Sr_xVO_3$, $Sr_{1-x}Y_xTiO_3$, and $La_{1-x}Sr_xCr_{0.5}Mn_{0.5}O_3$ have shown improved sulfur tolerance.[12–16] However, due to reasons such as poor catalytic activity toward fuel oxidation, low electrical conductivity, and inadequate compatibility with other cell components, none of these materials can satisfy all the practical requirements for SOFCs.

Other approaches to improve the sulfur tolerance through the controlled surface modification on the entire Ni-YSZ surface with NbO_2, CeO_2 and $Sm_{0.2}Ce_{0.8}O_2$ have also been introduced.[17–19] A thin layer of ceria and/or NbO_2 on Ni-YSZ appears to behave as a sulfur sorbent through the formation of oxysulfide, while the sulfur adsorbed on the uncovered Ni surface is extremely stable and desorbed only at temperature above 1230°C. With surface modification, however, ceria and Nb particles are deposited randomly by multiple infiltration steps and the Ni-YSZ anode pores can be blocked by these catalysts. This pore size reduction has been shown to cause mass flow limitations in the electrodes. Therefore, proper surface modification of the anode backbone with a continuous thin-film coating on the Ni-YSZ surface is critical to obtain stable performance.

Ni-$BaZr_{0.1}Ce_{0.7}Y_{0.1}Yb_{0.1}O_{3-\delta}$ (BZCYYb) composites recently have been studied as anodes, due to their high catalytic activity, coke resistance, and ability to use H_2S containing fuel with minimum degradation.[1] Ni-BZCYYb shows no performance loss in power output upon exposure to H_2S contaminated fuels, and appears to be the most preferable anode identified thus far. However, Ni-BZCYYb readily reacts with YSZ at high temperature to form an electronically insulating phase, which hinders O^{2-} ion conducting paths in the YSZ electrolyte. The aforementioned materials thus cannot fully satisfy requirements for applicability to state-of-the-art Ni-YSZ fuel cell systems.

In the present study, we report findings on the surface modification of a Ni-YSZ anode using BZCYYb to enhance the sulfur tolerance of anode. We show that only a single-step infiltration of BZCYYb significantly improves the sulfur tolerance of the Ni-YSZ anode over long periods of time. Furthermore, to investigate the behavior of the SOFC anode after the operation on a sulfur contaminated fuel, the modified Ni-YSZ anode before and after exposure to the sulfur contaminated fuel is characterized thorough Raman spectroscopy. The stability of the Ni-YSZ anode is discussed with regard to the amount of BZCYYb infiltration, based on a long term electrochemical stability test and ex-situ Raman spectroscopy analysis.

Experimental

A BZCYYb solution was prepared using quantitative amounts of metal precursors $Ba(NO_3)_2$ (Sigma-Aldrich), $ZrO(NO_3)_2 \cdot 4H_2O$ (Alfa Aesar), $Ce(NO_3) \cdot 6H_2O$ (Sigma-Aldrich), Y_2O_3 (Alfa Aesar), and Yb_2O_3 (Alfa Aesar). First, Y_2O_3 and Yb_2O_3 were dissolved in HNO_3, and then $ZrO(NO_3)_2 \cdot 4H_2O$ was added to the solution with stirring and heating on a hot plate. After the solution became clear, $Ba(NO_3)_2$, and $Ce(NO_3)_3 \cdot 6H_2O$ were then added. Citric acid was added in a 1:1 metal ions: citric acid molar ratio and the pH value was adjusted to about 7 with $NH_3 \cdot H_2O$ to obtain a stable BZCYYb solution. A X-ray diffraction (XRD) analysis was used to examine the phase formation of the BZCYYb powder (derived from the BZCYYb solution) as well as the chemical compatibility between BZCYYb and YSZ.

In order to study the morphology of the BZCYYb coating on the Ni-YSZ anode surface, dense Ni-YSZ pellets were used as substrates to facilitate the observation. The dense Ni-YSZ composite pellets were prepared by ballmilling a mixture of Ni powder (~300 mesh, Alfa Aesar) and YSZ (Tosoh) at a volume ratio of 50:50 in ethanol for 12 h. The dried powders were pressed into pellets in a 13 mm diameter die and the pressed pellets were sintered at 1400°C for 4 h in 10 vol% H_2 balanced by N_2. The sintered pellets were mechanically polished to obtain a smooth surface finally. 5 μL BZCYYb solutions with different concentrations, 0.2 M, and 0.1 M, were then coated on the polished Ni-YSZ surface using a micro-liter syringe to control the

*Electrochemical Society Fellow.
zE-mail: gtkim@unist.ac.kr; jyshin@deu.ac.kr

Downloaded on 2014-04-21 to IP 128.61.136.152 address. Redistribution subject to ECS terms of use (see ecsdl.org/site/terms_use) unless CC License in place (see abstract).

amount of loading. After being dried in air, the BZCYYb coated Ni-YSZ pellets were fired at 950°C in 10% H_2/90% N_2 for 4 h and cooled to room temperature for further analysis. The surface morphology of the BZCYYb coated pellets was examined using scanning electron microscopy (SEM).

For ex-situ Raman spectroscopy, unmodified Ni-YSZ and BZCYYb coated pellets were sealed in an alumina tube furnace and heated to 800°C in a 50 ppm H_2S-H_2 gas mixture for 18 h. The samples were then examined at room temperature using Raman microspectroscopy (WITec, Helium Neon Laser 532 nm).

To evaluate the BZCYYb modification process under fuel cell operating conditions, electrolyte supported cells were fabricated with a configuration of Ni-YSZ/YSZ/SDC/LSCF. First, the NiO-YSZ anode and YSZ electrolyte were tape-casted separately, as reported elsewhere.[3,12] The electrolyte supported NiO-YSZ/YSZ was then prepared by lamination, followed by sintering at 1450°C for 5 h to densify the YSZ electrolyte. A $Sm_{0.2}Ce_{0.8}O_{2-\delta}$ buffer layer was deposited on the YSZ electrolyte surface. $La_{0.6}Sr_{0.4}Co_{0.2}Fe_{0.8}O_{3-\delta}$ (LSCF) cathode powders prepared by the Pechini method were mixed with V-006 and acetone to form a cathode slurry, which was screen-printed on the YSZ electrolyte, followed by firing at 1000°C for 4 h. The final thickness of the anode and the electrolyte was 150 μm and 100 μm, respectively, with an anode active area of 0.36 cm^2. 5 μL BZCYYb solutions with different concentrations, 0.2 M, and 0.1 M, were then infiltrated on the NiO-YSZ electrolyte supported cell (3.5 wt% BZCYYb) and sintered in air at 950°C for 4 h. NiO paste and Ag paste were used as the current collector in the anode and cathode, respectively. For a single cell performance test, the cell was mounted on an alumina tube with ceramic bond (Ceramabond 522, Aremco). The cell was placed inside an electrical furnace and heated to 700°C. The anode was exposed to pure H_2 and H_2S containing H_2 at a flow rate of 50 mL min^{-1}. The cell performance was monitored using a BioLogic Potentiostat, in galvanostatic mode, i.e., monitoring the cell voltage at constant current.

Results and Discussion

BZCYYb powders derived from the BZCYYb solution were prepared to characterize the crystalline phase of the BZCYYb films coated on Ni-YSZ anodes. The XRD patterns of BZCYYb-YSZ (1:1 wt% mixture) calcined in air at different temperatures are presented in Figure 1a, and suggest that there was no evidence of a solid state reaction between BZCYYb and YSZ at temperatures below 950°C. Figure 1b shows the XRD patterns for the BZCYYb powder calcined at 950°C in air and in a H_2 atmosphere. From the XRD patterns, it is clear that BZCYYb is stable under both oxidizing and reducing conditions. The XRD patterns of BZCYYb at room temperature reveal sharp perovskite peaks without any additional peaks corresponding to other phases.

Figures 2a, 2b display SEM images of a polished surface of dense Ni-YSZ pellets. The Ni-YSZ dense pellet was used to study the morphology of the BZCYYb coating on the Ni-YSZ surface. Figure 2c, 2d, and 2e show SEM images of 0.2 M (5 μL) BZCYYb coated Ni-YSZ pellets. Figure 3a, 3b shows the morphology of 0.1 M (5 μL) BZCYYb coated Ni-YSZ pellets. Compared with the unmodified Ni-YSZ pellet, 0.2 M BZCYYb coated pellets show nano-scale BZCYYb particles which were mostly observed on the Ni surface rather than on the YSZ surface. The BZCYYb particles appear to preferentially coat the Ni surface; a fairly non-uniform coating of BZCYYb particles with a size of ~100 nm (Figure 2d) was obtained. The BZCYYb catalyst nanoparticles partly cover the Ni surfaces and allow a significant fraction of triple phase boundaries (TPB) at the Ni-YSZ junctions. Notably, the BZCYYb modification may allow extension of TPBs so that some of the Ni surface can participate in the electrochemical reaction. In contrast, other modification processes require a fully covered Ni-YSZ surface, which may decrease the number of electrochemical reaction sites.

Figure 4a shows an optical micrograph of a Ni-YSZ polished pellet. Similar to the SEM image, the optical micrograph shows Ni regions as bright color and YSZ regions as dark gray color, respectively. Figure 4b shows the corresponding Raman spectra of the clean Ni-YSZ anode surface. The Raman spectrum for the YSZ polycrystalline region has a Raman shift peak at 622 cm^{-1} and weaker bands at 491 cm^{-1}.[9] On the other hand, in the Raman spectrum for the Ni region, no anomalous Raman signal is detected and the spectrum is essentially featureless. Figure 4c and 4d show an optical micrograph and Raman spectra of Ni-YSZ pellets exposed to a fuel mixture of 50 ppm H_2S-H_2 for 18 h at 800°C, respectively. The Raman spectra for Ni regions exposed to H_2S show a sharp band at 399 cm^{-1} and several weaker bands at 192 cm^{-1}, 214 cm^{-1}, 299 cm^{-1}, and 318 cm^{-1}, corresponding to Ni_3S_2.[9] A close examination of the Ni surface by Raman spectra shows that Ni was well covered by Ni_3S_2. Meanwhile, the Raman spectra for YSZ regions have no observable change, suggesting that H_2S does not contaminate the YSZ. The Ni_3S_2 identified in this work was formed during the cooling process, as the in-situ analysis shows that Ni_3S_2 is unstable under typical SOFC operating conditions.[9]

Figure 4 display an optical micrograph and Raman spectra collected from a 0.2 M (Fig. 4e, 4f) and 0.1 M BZCYYb (Fig. 4g, 4h) modified Ni-YSZ pellet following exposure to a fuel mixture of 50 ppm H_2S containing H_2 gases for 18 h at 800°C, respectively. As expected, the acquired Raman spectra consist of similar features of uncontaminated Ni-YSZ, as shown in Figure 4, confirming that sulfur contamination does not occur on the BZCYYb modified Ni-YSZ surface. Raman spectra for the modified sample were collected point-by-point from all regions of the Ni-YSZ pellets. The Raman spectra

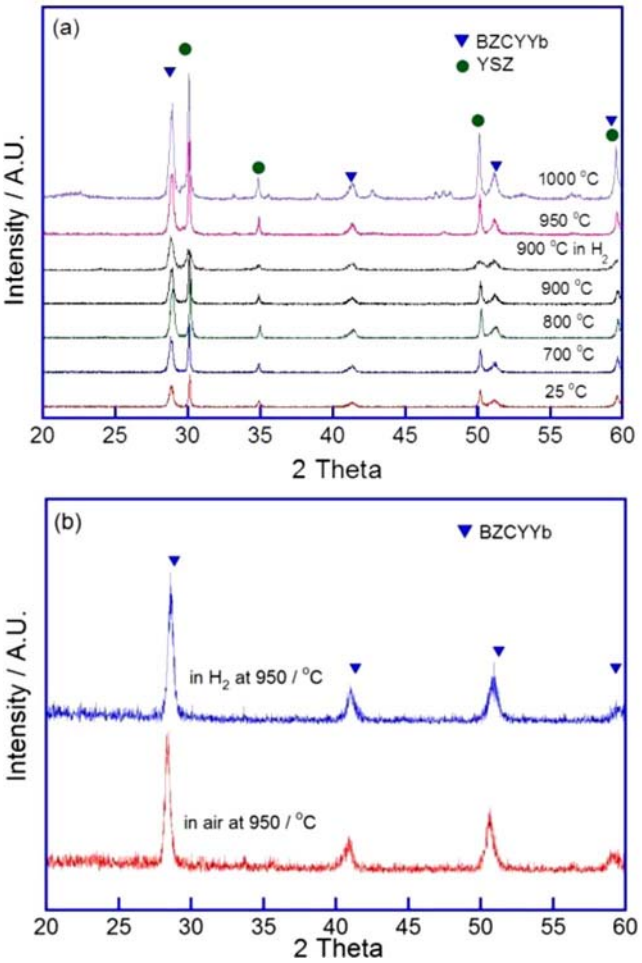

Figure 1. **(a)** XRD patterns of BZCYYb-YSZ (50/50 by weight %) sintered in air at 25–1000°C and in H_2 at 900°C for 4 h. **(b)** XRD patterns of BZCYYb prepared in air and H_2 at 950°C for 4 h.

Downloaded on 2014-04-21 to IP 128.61.136.152 address. Redistribution subject to ECS terms of use (see ecsdl.org/site/terms_use) unless CC License in place (see abstract).

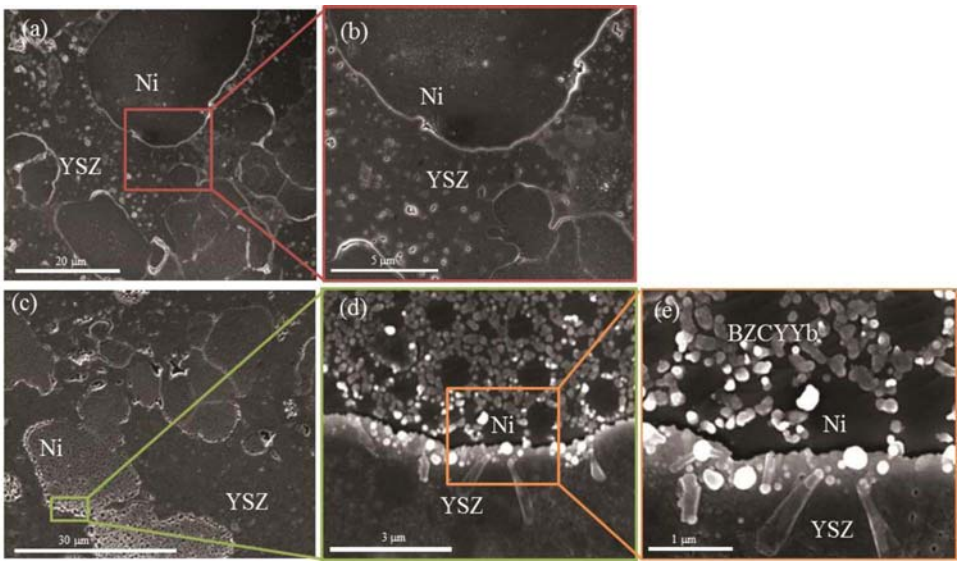

Figure 2. A high-resolution SEM image of **(a, b)** Ni-YSZ, and **(c, d, e)** 0.2 M BZCYYb Ni-YSZ.

collected from Ni-YSZ show that significant tolerance exists only in the presence of the BZCYYb catalyst.

Figure 5a shows the cross section SEM image of 0.2 M BZCYYb Ni-YSZ/YSZ/LSCF electrolyte supported cell. As shown in the SEM images of 0.2 M (5 μL) BZCYYb modified NiO-YSZ (Figure 5b, 5c), the BZCYYb nano scale particles are mostly observed on the NiO surface rather than on the YSZ surface. Figure 6a and 6b shows the electrochemical performance of Ni-YSZ/YSZ/LSCF and 0.2 M BZCYYb Ni-YSZ/YSZ/LSCF. The 0.2 M BZCYYb Ni-YSZ and Ni-YSZ anodes were exposed to 30 ppm and 20 ppm H_2S-H_2 fuel, respectively, after the cell was stabilized at 700°C in H_2 and the cell voltage was measured under a constant current of −0.054 Acm^{-2}. Figure 7a and 7b shows the electrochemical performance of 0.2 M BZCYYB Ni-YSZ/YSZ/LSCF and 0.1 M BZCYYb Ni-YSZ/YSZ/LSCF cells in 20–100 ppm H_2S containing H_2 fuel at 700°C under a constant current of −0.054 Acm^{-2}. Immediately after exposure to 20 ppm H_2S containing H_2 fuel, the cell voltage of the unmodified Ni-YSZ anode dropped to 620 mV. The cell performance of the unmodified Ni-YSZ anode gradually decreased under 20 ppm H_2S at 700°C and completely degraded after 25 hours of H_2S contamination. The cell with 0.2 M BZCYYb modified Ni-YSZ anode, however, shows a remarkably stable perfomance in 30 ppm H_2S without any degradation for 500 hours. For the cell with BZCYYb modification, the initial cell voltage (810 mV) was higher than that (730 mV) of the unmodified anode at a constant current density of −0.054 Acm^{-2}.

In this study, the unique microstructure of the BZCYYb modified anode prepared by the infiltration approach has two notable advantages compared to the anodes prepared via other modification processes.[15–17] First, only a single-step of BZCYYb infiltration is sufficient to assure good sulfur tolerance. Second, the nano-sized BZCYYb particles appear to be distributed only on the Ni surface, and thus effective TPB sites are preserved, where oxygen ions, electrons, and fuel meet.

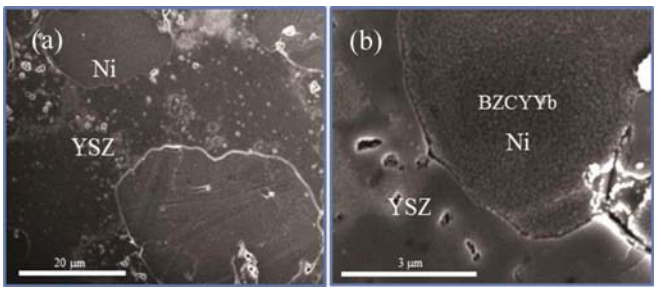

Figure 3. A high-resolution SEM image of (**a, b**) 0.1 M BZCYYb Ni-YSZ.

In sulfur containing fuels, sulfur poisoning occurs due to the strong absorption of elemental sulfur on the Ni surface, which blocks the TPBs.[20] For an unmodified Ni-YSZ anode, sulfur absorption (Equation 1) on the Ni surface and the removal process (Equation 2) can be expressed as,

$$H_2S + Ni \rightarrow S_{Ni}{}^{*} + H_2 \quad [1]$$

$$S_{Ni}{}^{*} + 2O^{2-} \rightarrow Ni + SO_2 + 4e^{-} \quad [2]$$

where $S_{Ni}{}^{*}$ denotes sulfur absorbed on the Ni surface and TPB. For an unmodified Ni-YSZ anode, the elemental sulfur absorbed on the Ni surface cannot be removed by reaction (Equation 2), since this reaction (Equation 2) is expected to be slow due to (a) a larger amount of elemental sulfur blocking the TPB sites and (b) a larger number of electrons involved. Considering the blockage of the TPB sites by sulfur and the large number of electrons involved, reaction 2 may be the rate determining step for the recovery process when the fuel is switched back to clean H_2. This recovery process, i.e., reaction 2, may not be 100% completed due to the microstructural change of the Ni-YSZ anode.[15]

On the other hand, the improved sulfur tolerance of the 0.2 M BZCYYb modified Ni-YSZ anode may be related to the water uptake property of proton conducting materials, $BaZrO_3$-$BaCeO_3$.[1] Figure 8 shows the weight change observed for BZCYYb powder samples upon exposure to humidifyed argon at 750°C. Recent studies have shown that BZCYYb, BaO, $BaZr_{1-x}Y_xO_3$, and $BaZr_{1-x}Yb_xO_3$ materials have outstanding coking tolerance and sulfur tolerance due to their absorbed or adsorbed water uptake property at the microscopic level.[1,3,21,22] The actual sulfur removal mechanism of the BZCYYb modified Ni-YSZ anode is still unclear, but it can be hypothesized as illustrated in Figure 9. The adsorbed sulfur on the Ni surface may be removed by a simpler pathway, which is the direct reaction of absorbed water on BZCYYb with absorbed sulfur on the Ni surface. The sulfur tolerance of the modified BZCYYb Ni-YSZ anode may be a three step chemical process and can be summarized as shown in Figure 9. Step 1: the absorption of elemental sulfur in the Ni-YSZ surface, which blocks the TPB sites (Equation 1). Step 2: interaction of absorbed water on BZCYYb with the elemental sulfur at TPB. Step 3: formation of SO_2 or removal of sulfur from the TPB region. Also, the morphology of the 0.2 M BZCYYb modified Ni-YSZ anode (Figure 2) shows that

Downloaded on 2014-04-21 to IP 128.61.136.152 address. Redistribution subject to ECS terms of use (see ecsdl.org/site/terms_use) unless CC License in place (see abstract).

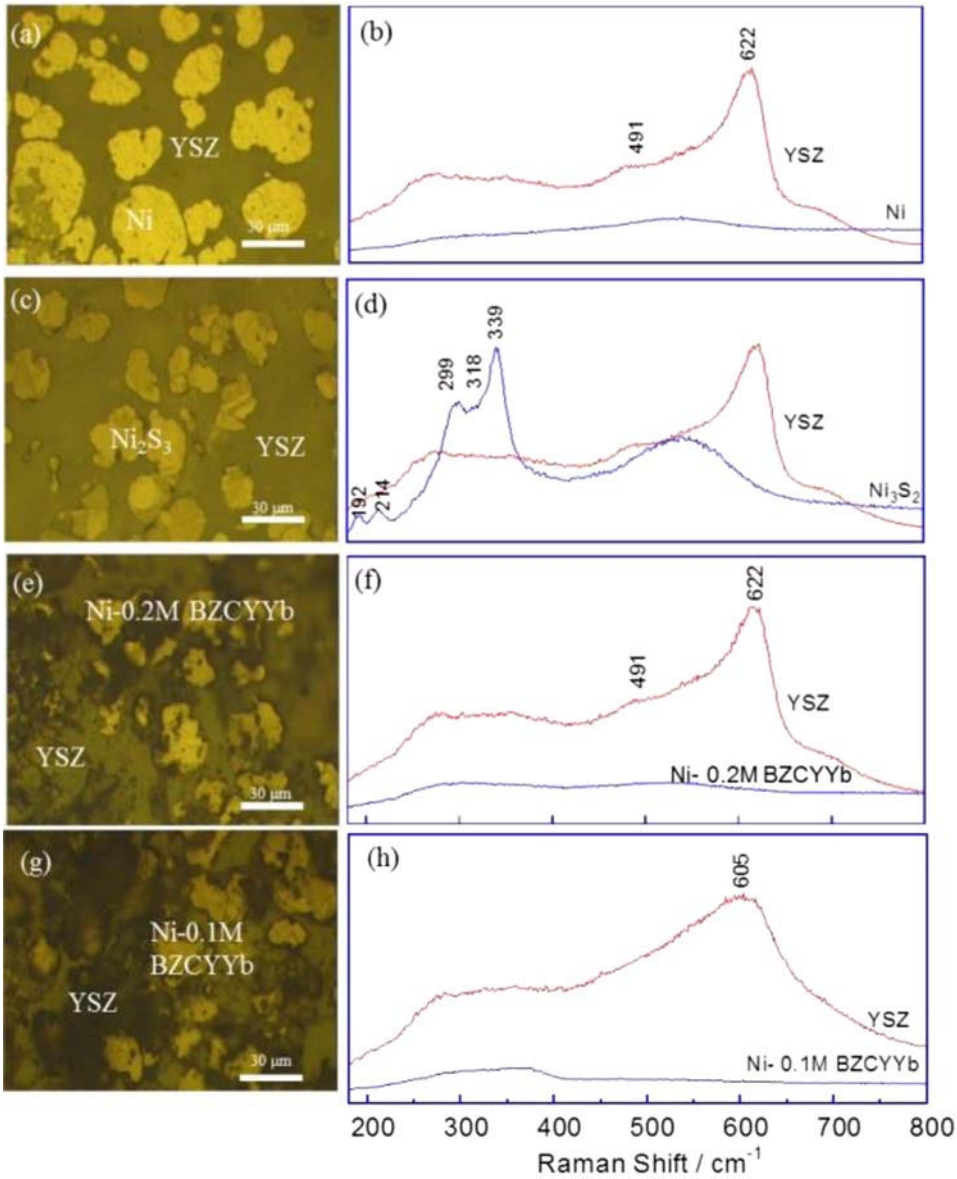

Figure 4. Optical micrograph of **(a)** clean Ni-YSZ anode surface, **(c)** Ni-YSZ pellet after exposure to 50 ppm H_2S-H_2, **(e)** 0.2 M BZCYYb and **(g)** 0.1 M BZCYYb modified Ni-YSZ composite after exposure to 50 ppm H_2S-H_2 at 800°C for 18 h. Corresponding Raman spectra of the clean **(b)** Ni-YSZ anode surface, **(d)** Ni-YSZ polished pellet after exposure to 50 ppm H_2S-H_2, **(f)** 0.2 M BZCYYb and **(h)** 0.1 M BZCYYb modified Ni-YSZ composite after exposure to 50 ppm H_2S-H_2 at 800°C for 18 h. The bright color in the optical micrographs shows Ni regions and gray-dark color shows YSZ regions.

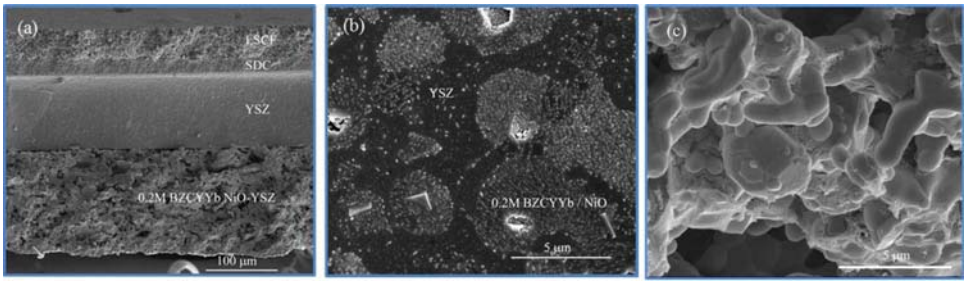

Figure 5. A high-resolution SEM image of **(a)** 0.2 M BZCYYb modifyed NiO-YSZ electrolyte supported cell, and **(b)** 0.2 M BZCYYb NiO-YSZ dense pellet **(c)** 0.2 M BZCYYb infiltrated porous NiO-YSZ cell.

Downloaded on 2014-04-21 to IP 128.61.136.152 address. Redistribution subject to ECS terms of use (see ecsdl.org/site/terms_use) unless CC License in place (see abstract).

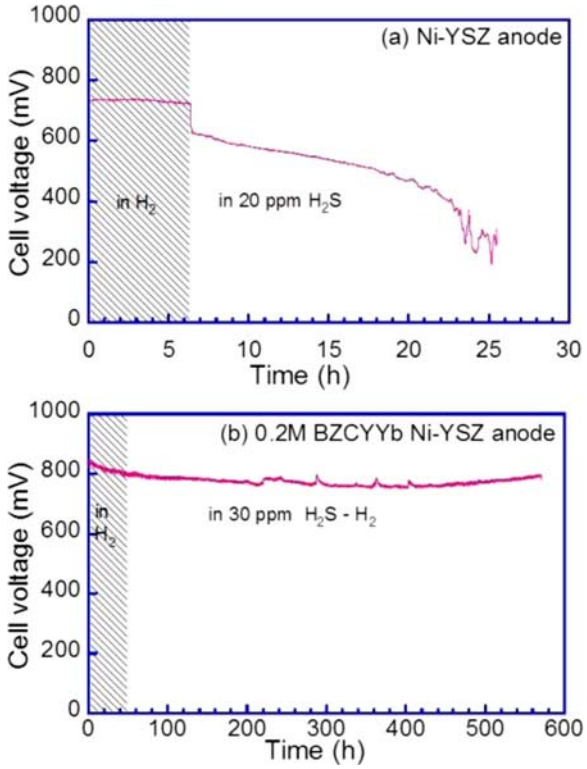

Figure 6. **(a)** Shows the electrochemical performances of Ni-YSZ anode (3% H_2O) H_2 and 20 ppm H_2S balanced with H_2 at 700°C under a constant current load of −0.054 A cm^{-2}. **(b)** shows the electrochemical performances of 0.2 M BZCYYb Ni-YSZ anode (3% H_2O) H_2 and 30 ppm H_2S balanced with H_2 at 700°C under a constant current load of −0.054 A cm^{-2}.

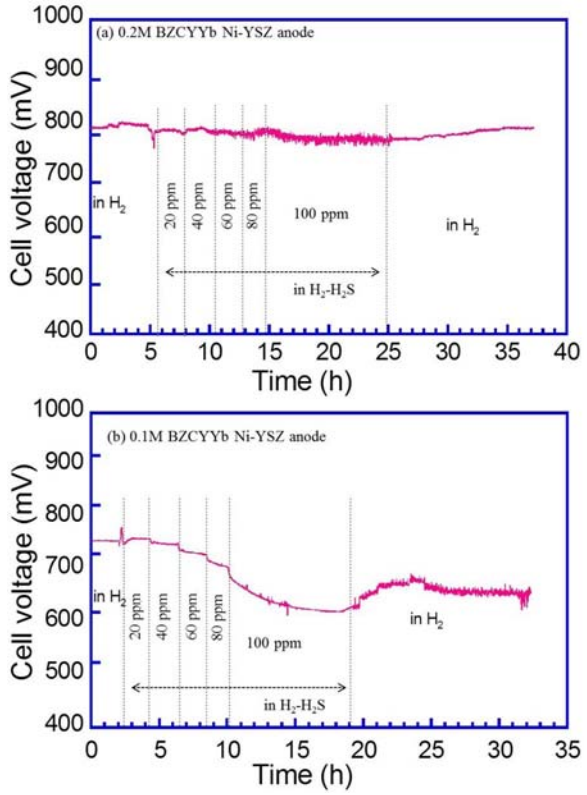

Figure 7. Electrochemical performances of (a) 0.2 M BZCYYb Ni-YSZ anode and (b) 0.1 M BZCYYb Ni-YSZ anode in (3% H_2O) H_2 and 20–100 ppm H_2S balanced with H_2 at 700°C under a constant current load of −0.054 A cm^{-2}.

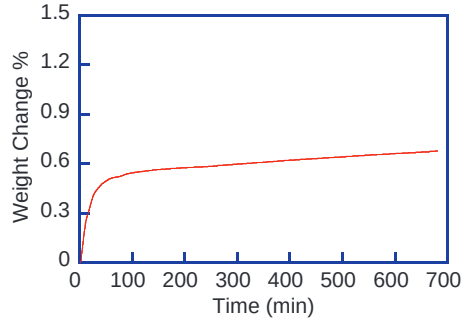

Figure 8. Typical thermogravimetric traces for BZCYYb powder samples in wet argon 750°C.

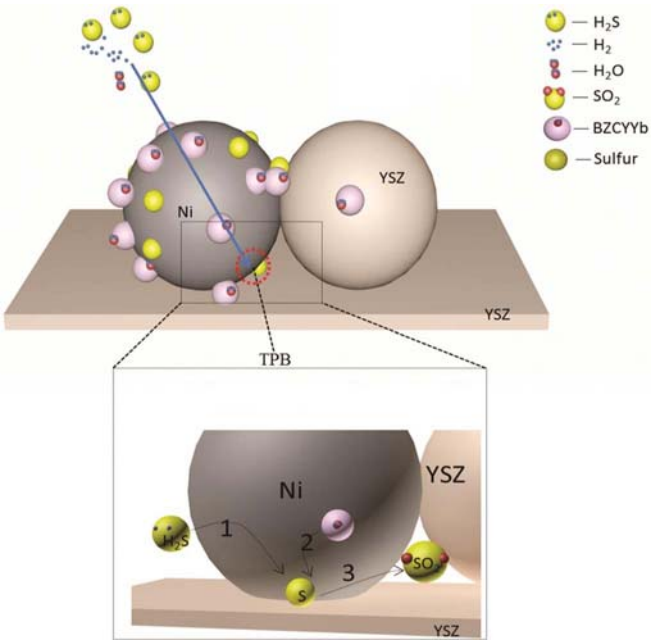

Figure 9. Schematic showing the anodic reaction pathways for the 0.2 M BZCYYb Ni-YSZ / YSZ anode structure under SOFC operating conditions. The three step sulfur removal processes are as follows: **Step 1:** absorption of elemental sulfur in Ni surface, **Step 2:** interaction of absorbed water on BZCYYb with the elemental sulfur and **Step 3:** removal of sulfur from the Ni surface.

BZCYYb particles are mostly decorated on the Ni surface, which helps remove the adsorbed sulfur without blocking TPB sites. These results indicate that BZCYYb modified Ni-YSZ anodes could be used for operation with sulfur containing fuels. A single-step infiltration of BZCYYb leads to significant sulfur tolerance for a long period of time on a conventional Ni-YSZ anode.

Conclusions

A BZCYYb sulfur tolerant nanocoating, produced by a simple and economic infiltration method, on the conventional Ni-YSZ based SOFC anodes shows notably stable performance over 500 h, in humidified H_2 containing 30 ppm H_2S. The electrolyte supported cell with the BZCYYb modified Ni-YSZ anode shows stable performance under an applied current of −0.054 Acm^{-2} at 700°C in a significant concentration of sulfur, whereas the unmodified Ni-YSZ anode was contaminated by H_2S, which causes electrochemical degradation. The present work demonstrates the importance of BZCYYb, as well as morphology control, to achieve stable performance of Ni-YSZ in sulfur containing fuels. Surface modification of Ni-YSZ by BZCYYb provides stable electrochemical performance in sulfur containing fuels for a long time. The BZCYYb modified anodes are feasible for

Downloaded on 2014-04-21 to IP 128.61.136.152 address. Redistribution subject to ECS terms of use (see ecsdl.org/site/terms_use) unless CC License in place (see abstract).

the steady operation at the intermediate operating temperatures as a crucial element of the state-of-the-art Ni-YSZ fuel cell systems.

Acknowledgments

This research was supported by the New & Renewable Energy of the Korea Institute of Energy Technology Evaluation and Planning (KETEP) (20113020030060) grant funded by the Korea government Ministry of Knowledge Economy, the Development Program of the Korea Institute of Energy Research (KIER)(B4-2424), the Basic Science Research Program (2010-0021214 & 2012R1A1A1013380) funded by the Ministry of Science, ICT and Future Planning, and the BK21 plus (10Z2013001105) funded by the Korea government Ministry of Education.

References

1. L. Yang, S. Wang, K. Blinn, M. Liu, Z. Liu, Z. Cheng, and M. Liu, *Science*, **326**, 126 (2009).
2. S. C. Singhal, *Solid State Ionics*, **135**, 305 (2000).
3. M. Liu, Y. Choi, L. Yang, K. Blinn, W. Qin, P. Liu, and M. Liu, *Nano Energy*, **1**, 448 (2012).
4. M. L. Toebes, J. H. Bitter, A. J. Dillen, and K. P. Jong, *Catal. Today.*, **76**, 33 (2002).
5. M. Liu, M. E. Lynch, K. Blinn, F. M. Alamgir, and Y. Choi, *Materials Today*, **14**, 534 (2011).
6. Z. Cheng, S. Zha, and M. Liu, *J. Power Sources*, **172**, 688 (2007).
7. K. Sasaki, K. Susuki, A. Iyoshi, M. Uchimura, N. Imamura, H. Kusaba, Y. Teraoka, H. Fuchino, K. Tsujimoto, Y. Uchida, and N. Jingo, *J. Electrochem Soc.*, **153**, A2023 (2006).
8. Y. Matsuzaki and I. Yasuda, *Solid State Ionics*, **132**, 261 (2000).
9. Z. Cheng and M. Liu, *Solid State Ionics*, **178**, 925 (2007).
10. Y. M. Choi, C. Compson, M. C. Lin, and M. Liu, *Chem Phys Lett.*, **421**, 179 (2006).
11. S. W. Zha, Z. Cheng, and M. L. Liu, *J. Electrochem Soc.*, **154**, B201 (2007).
12. G. Kim, G. Corre, J. T. S Irvine, J. M. Vohs, and R. J. Gorte, *Electrochem Solid State Lett.*, **11**, B16 (2008).
13. Y.-H. Huang, R. I. Dass, J. C. Denyszyn, and J. B. Goodenough, *J. Electrochem Soc.*, **153**, A1266 (2006).
14. Z. Cheng, S. Zha, L. Aguilar, D. Wang, J. Winnick, and M. Liu, *Electrochem Solid State Lett.*, **9**, A31 (2006).
15. M. Cooper, K. Channa, R. De Silva, and D. J. Bayless, *J. Electrochem Society.*, **157**, B1713 (2010).
16. A. Torabi and T. H. Etsell, *J. Power Sources*, **225**, 51 (2013).
17. S. Choi, J. Wang, Z. Cheng, and M. Liu, *J. Electrochem Society.*, **155**, B449 (2008).
18. J. W. Yun, H. C. Ham, H. S. Kim, S. A. Song, S. W. Nam, and S. P. Yoon, *J. Electrochem Society.*, **160**, F153 (2013).
19. J. W. Yun, S. P. Yoon, J. Han, S. Park, H. S. Kim, and S. W. Nam, *J. Electrochem Society.*, **157**, B1825 (2010).
20. W. G. Bessler, M. Vogler, H. Stormer, D. Gerthsen, A. Utz, A. Weber, and E. I Tiffee, *Phys Chem Chem Phys.*, **12**, 13888 (2010).
21. K. S. Blinn and M. Liu, *J. Power Sources.*, **243**, 24 (2013).
22. K. S. Blinn, H. Abernathy, X. Li, M. Liu, L. A. Bottomley, and M. Liu, *Energy Environ Sci.*, **5**, 7913 (2012).

Downloaded on 2014-04-21 to IP **128.61.136.152** address. Redistribution subject to ECS terms of use (see **ecsdl.org/site/terms_use**) unless CC License in place (see abstract).